

PACS numbers: 52.38.Mf; 61.80.Ba
DOI: 10.1070/QE2003v033n09ABEH002499

On possible manifestations of the induced transparency during laser evaporation of metals

S.N. Andreev, V.I. Mazhukin, N.M. Nikiforova, A.A. Samokhin

***Abstract*. The possible acoustic and optical manifestations of the induced transparency during laser evaporation of metals are analysed. It is shown that under certain conditions the photoacoustic effect related to the movement of the induced-transparency front can make an appreciable contribution to the total recoil pressure. The formation of the induced-transparent layer can be accompanied at the initial instant of time by both the decrease and the increase in the reflectance of the target. It is established that the laser intensity, required to realise the stationary regime of evaporation with induced transparency, is substantially lower than the threshold of plasma formation.**

Keywords: *laser evaporation, photoacoustic effect, induced transparency, explosive boiling.*

1. Introduction

Phase transitions from liquid to vapour, taking place upon quasi-equilibrium evaporation of metals, are accompanied by metal – insulator transitions, since for many metals at temperatures below the critical liquid – vapour temperature the equilibrium degree of ionisation of vapours turns out to be rather small because the ionisation potential is comparatively high with respect to the critical temperature T_c.

As the temperature increases, the metal density decreases and a metal – insulator transition can, in principle, take place in a condensed phase at a temperature $T_{md} < T_c$, which was for the first time noticed in Ref. [1]. It is evident that such a transition will be accompanied by a drastic decrease in the absorption coefficient, i.e., by an increase in the depth of the laser radiation penetration into the target.

Such induced transparency was discussed in Refs [2 – 5] in connection with the results of irradiation of lead and bismuth targets by millisecond Nd : YAG-laser pulses. The question, concerning the origin of induced transparency in the experiments [2], was at that time left open for a number of reasons (such as the spatio-temporal inhomogeneity of the laser pulse, the lack of data on the variation of the recoil pressure during target exposure and others), complicating an unambiguous interpretation of experimental results [2]. As far as we know, no reports on experimental results of this kind for millisecond exposures were made ever since, although different problems of the laser-induced evaporation and explosive boiling were investigated in many works (see, for example, Refs [6 – 16]). The authors of recent work [17] carried out the experiments on the exposure of silicon, which transforms into metal when melting, to laser radiation ($\lambda = 266$ nm, $I_0 = 10^9 - 10^{11}$ W cm^{-2}), and revealed a dramatic (more than by an order of magnitude) increase in the crater depth at intensities $I \geqslant 2.2 \times 10^{10}$ W cm^{-2}. The main removal of mass in their research occurred at the time delay of approximately 300 ns after irradiation by a 3-ns laser pulse.

The authors of Ref. [17] interpreted the observed effect as induced transparency of the material of the irradiated target, which provides deep penetration of laser radiation into the target, with the subsequent explosive boiling of the superheated liquid phase. Some aspects of this interpretation were discussed also in Refs [18, 19]. It should be noted that the formation of the layer, transparent for laser radiation, with optically sharp boundaries was observed in experiments on irradiation of metals and semiconductors by femtosecond pulses, and this layer existed for about 1 ns [20 – 23].

A sharp (tens of times) increase in the crater depth, observed in Ref. [17], is a serious argument in favour of the interpretation, proposed by the authors of this work. However, in later work [24], devoted to the same problem and accomplished by almost the same co-authors, the induced transparency is no more used to explain the drastic increase in the crater depth; instead, an attempt to attribute this increase to the heat-conduction process and subsequent explosive boiling after the end of the laser pulse is made. As mentioned above, such an ambiguity of interpretations of the results arises particularly from the deficiency in the experimental data. To study this effect in detail, a complex experimental diagnostics including optical, acoustical and other measurements is required.

In this connection, a more detailed theoretical study of particularities of the laser evaporation regime in the presence of the induced transparency in the irradiated matter is of interest for stimulating the appropriate experiments. Such a study is the main goal of this work.

S.N. Andreev, A.A. Samokhin A.M. Prokhorov General Physics Institute, Russian Academy of Sciences, ul. Vavilova 38, 119991 Moscow, Russia; e-mail: andreev@nccom.ru, asam@ran.gpi.ru;
V.I. Mazhukin Institute for Mathematical Modelling, Russian Academy of Sciences, Miusskaya pl. 4a, 125047 Moscow, Russia;
N.M. Nikiforova Department of Physics, M.V. Lomonosov Moscow State University, Vorob'evy Gory, 119992 Moscow, Russia

Received 23 January 2003
Kvantovaya Elektronika **33** (9) 771 – 776 (2003)
Translated by Yu.M. Mikhailova

2. Stationary and 'semi-stationary' regimes of evaporation

We will describe the evolution of the temperature distribution inside the evaporated target using a one-dimensional time-dependent heat-conduction equation, taking into account the possibility of an abrupt change in the optical and thermal parameters of the target matter [25]. In the coordinate system, the origin of which is attached to the evaporation front, moving at the velocity V through the static material in the positive direction of the z axis in the laboratory reference frame, this equation has the form

$$\frac{\partial T}{\partial t} - V\frac{\partial T}{\partial z} = \chi\frac{\partial^2 T}{\partial z^2} + \frac{\alpha I}{c\rho}\mathrm{e}^{-\alpha z}, \tag{1}$$

where χ, α, c and ρ are the thermal conductivity, absorption coefficient, specific heat, and density of the target material, respectively; $I = I_{\mathrm{las}}\eta(1-R)$ is the absorbed intensity; R is the reflection coefficient of the material. The coefficient $\eta \leqslant 1$ accounts for the possible attenuation of the incident laser radiation I_{las} in the near-surface plasma layer.

When the induced-transparency (bleaching) temperature T_{b} is achieved and a sufficiently sharp change in α and χ takes place, a layered structure, schematically represented in Fig.1, appears in the irradiated target. Inside each of layers, the temperature profile is determined by Eqn (1) with values of the absorption coefficient α_i and thermal conductivity χ_i corresponding to this layer and conditions of continuity of the temperature and heat flow, taking into account the heat of the corresponding phase transition at layer boundaries. Note that the boundary of the induced-transparent layer does not necessary coincide with the evaporation surface, since the near-surface layer can remain non-transparent under appropriate conditions due to the evaporation cooling.

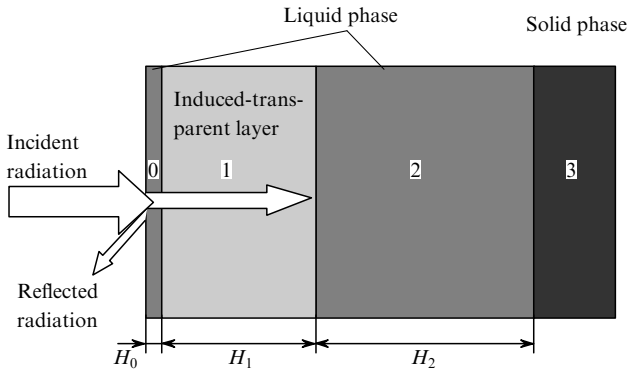

Figure 1. Schematic view of the irradiated target in the presence of induced transparency: (0) near-surface non-transparent liquid layer, (1) induced-transparent layer, (2) second non-transparent liquid layer, (3) semi-infinite solid phase.

The evaporation front velocity V and recoil pressure p_{v}, which depend on the surface temperature T_{s} and the Mach number M of the flow of evaporated matter, are

$$V = K_1 V_0, \quad p_{\mathrm{v}} = K_2 p_{\mathrm{s}}, \tag{2}$$

where $V_0 = [m/(2\pi k T_{\mathrm{s}})]^{1/2}(p_{\mathrm{s}}/\rho)$; k is the Boltzmann constant; m is the target molecule mass. In accordance with one of the simplest models of the Knudsen layer [26], the values K_1 and K_2 can be represented as $K_1 = 1 - r^8$ and $K_2 = (1 + r^9)/2$, where the parameter r depends on the Mach number M. For $M = 1$ the parameters $r = 0.78$, $K_1 = 0.86$ and $K_2 = 0.56$ [26]. The dependence of the saturation pressure p_{s} on the surface temperature T_{s} is approximated by the formula

$$p_{\mathrm{s}} = p_0 \exp[A(1 - T_{\mathrm{v}}/T_{\mathrm{s}})], \tag{3}$$

where T_{v} is the temperature of boiling of the target matter under normal pressure $p_0 = 1$ bar and $A = 12$ is the constant.

In a stationary case, the solution of Eqn (1) within each layer has the form

$$T_i(z) = A_i + B_i\mathrm{e}^{-q_i z} + \frac{I_i}{c\rho\chi_i(q_i - \alpha_i)}\mathrm{e}^{-\alpha_i z}, \tag{4}$$

where $q_i = V/\chi_i$; the constants A_i and B_i are found from the boundary conditions at the surfaces separating induced-transparent and non-transparent layers, as well as liquid and solid phases. The subscript i ranges from 0 to 3 (see Fig. 1). The values of the absorbed intensities I_i within each layer are determined by the recurrent formula: $I_0 = I$, $I_{i+1} = I_i\mathrm{e}^{-\alpha_i H_i}$, where H_i is the thickness of the ith layer; $i = 0$, 1, 2. For simplicity, the possible influence of the interference is not taken into account in this formula.

The layer boundary conditions have the form

$$T_0 = T_{\mathrm{s}}, \quad \chi_0(\partial T_0/\partial z) = VL_{\mathrm{v}}/c \ \text{ for } \ z = 0, \tag{5}$$

$$T_0 = T_1 = T_{\mathrm{b}}, \ \chi_0(\partial T_0/\partial z) = \chi_1(\partial T_1/\partial z) \quad \text{for } z = H_0, \tag{6}$$

$$T_1 = T_2 = T_{\mathrm{b}}, \ \chi_1(\partial T_1/\partial z) = \chi_2(\partial T_2/\partial z) \quad \text{for } z = H_0 + H_1, \tag{7}$$

$$T_2 = T_3 = T_{\mathrm{m}}, \ \chi_2(\partial T_2/\partial z) = \chi_3(\partial T_3/\partial z) + VL_{\mathrm{m}}/c \quad \text{for } z = H_0 + H_1 + H_z, \tag{8}$$

$$T_3 = T_\infty, \quad \partial T_3/\partial z = 0 \quad \text{for} \quad z \to \infty,$$

where L_{v} is the latent vaporisation heat; T_{m}, L_{m} are, respectively, the temperature and latent melting heat of the target matter; and $T_\infty = 373$ K is the temperature of the solid phase at the sufficiently great depth. It is assumed in (6) and (7) that no appreciable absorption or heat release occurs at the induced-transparency front.

The typical form of the temperature profile for the silicon target is given in Fig. 2 for $I = 3.197 \times 10^7$ W cm^{-2}, $T_{\mathrm{b}} = 0.8T_{\mathrm{c}}$, $T_{\mathrm{c}} = 8000$ K, $T_{\mathrm{v}} = 3076$ K, $\alpha_0 = \alpha_2 = 1.13 \times 10^6$ cm^{-1}, $\alpha_1 = 100$ cm^{-1}, $\chi_0 = \chi_2 = 0.21$ cm^2 s^{-1}, $\chi_1 = \chi_0/10$. The rest parameters ($L_{\mathrm{m}} = 1797$ J g^{-1}, $L_{\mathrm{v}} = 13722$ J g^{-1}, $T_{\mathrm{m}} = 1683$ K, $c = 1.05$ J g^{-1} K^{-1}, $\rho = 2.52$ g cm^{-3}) are in close agreement with those given in Ref. [17].

In contrast to the regime considered in Ref. [17], where the temperature of the induced-transparent layer remains constant, in our case the temperature has the maximum

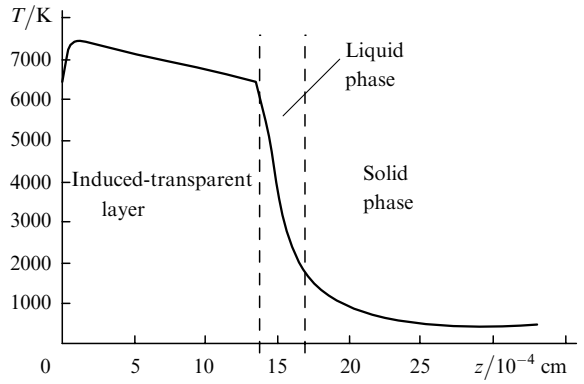

Figure 2. Typical view of the stationary temperature profile inside the silicon target in the presence of induced transparency for $I = 3.197 \times 10^7$ W cm^{-2}.

within the induced-transparent layer. The magnitude and position of this maximum depend on the parameters of the medium and laser pulse intensity [3]. For the threshold intensity $I_{th} = 3.1964 \times 10^7$ W cm^{-2}, the temperature of the induced transparency is achieved in a single point $z = H_0 = 0.84 \times 10^{-6}$ cm, i.e. the thickness H_1 of the induced-transparent layer is equal to zero. In this case, the layers 0 and 2 (see Fig. 1) adjoin, and the thickness H_0 of the near-surface non-transparent layer 0 is maximum.

As the intensity increases, the thickness H_1 of the induced-transparent layer increases, and H_0 tends to zero. For the intensity $I = 3.1976 \times 10^7$ W cm^{-2}, the maximum of the temperature profile reaches T_c, at this time $H_0 = 0.7 \times 10^{-6}$ cm and $H_1 = 19.7 \times 10^{-4}$ cm. The near-surface non-transparent layer disappears at the intensity $I_{max} = 3.273 \times 10^7$ W cm^{-2}, at which the maximum of the temperature profile exceeds the critical temperature by a factor of 2.3, which is beyond the bounds of applicability of the model with constant coefficients. The small value of the intensity range $\Delta I = I_{max} - I_{th}$ is connected in this case with the abrupt intensity-dependence of the temperature profile as well as with not very big difference between the induced-transparency temperature and critical temperature. With the increase in α_1, the range ΔI increases, the thickness of the induced-transparent layer (for the fixed value of the intensity I within the range ΔI) decreases.

The authors of Ref. [17] assumed, in fact, that when the induced-transparency temperature T_b is achieved, the absorption coefficient in the transparent medium becomes vanishingly small. In this case, the ordinary stationary regime of evaporation with the time-independent temperature profile in the system of evaporation front is not achieved, actually, in a one-dimensional model, because the front can penetrate arbitrarily deep into the target matter due to the absence of absorption in the induced-transparent layer. It is obvious that in such 'semi-stationary' regime, in contrast to the stationary one, the thickness of the induced-transparent layer will depend on the laser pulse duration.

At sufficiently high intensities, the velocity of the induced-transparency front V_1 can be appreciably greater than the velocity of the evaporation front V, which is maintained constant due to the absorption of laser radiation in the thin non-transparent layer, directly adjoining the evaporation border. The thickness of this layer can be determined from the expression

$$H_0 = \frac{1}{\alpha_0 - q_0} \ln\left(\frac{\alpha_0 I_0}{\alpha_0 I_0 - (\alpha_0 - q_0)\rho L_v V}\right), \quad (9)$$

which follows from the solution of Eqn (1) with the boundary condition (5) at a free surface $z = 0$ and conditions $T_0 = T_b$ and $(\partial T_0/\partial z) = 0$ at the induced-transparency boundary $z = H_0$, which provide invariability of the temperature within the induced-transparent layer.

At sufficiently high intensities I, the thickness H_0 of the near-surface non-transparent layer becomes too small, so that no macroscopic description can be applied. Nevertheless, independently on the method of description the absorption in the near-surface layer is a necessary condition for keeping such a regime, because in the induced-transparent layer the temperature profile $T = \text{const}$ does not provide heat supply, sufficient for keeping this evaporation regime. The necessity of the existence of the absorbing near-surface layer is also noted in Refs [2, 17].

3. Estimate of the influence of interference effects and plasma formation threshold

If the boundaries of the metal–insulator transition are sufficiently sharp and the condensed phase is sufficiently stable, the appearance of the induced transparency will be accompanied by the interference effects typical for the thin-film situation. The dependence of the coefficient of reflection of matter on thicknesses H_1 and H_0 of the transparent and non-transparent layers for $\lambda = 266$ nm is demonstrated in Fig. 3. Real and imaginary parts of the refraction coefficient of the induced-transparent and non-transparent matter were taken as $n_1 = 2.62$, $\xi_1 = 0.0002$, $n_0 = 11.7$ and $\xi_0 = 2.39$, which correspond to the values of coefficients of absorption $\alpha_1 = 100$ cm^{-1}, $\alpha_0 = 1.13 \times 10^6$ cm^{-1} and reflection $R_1 = 0.2$, $R_0 = 0.72$ for semi-infinite induced-transparent and non-transparent medium, which were used in Ref. [17]. As is seen from Fig. 3, the behaviour of the reflection coefficient R in the presence of the induced transparency is non-monotone and in some cases R can even exceed its initial value R_0.

Thus, in the case when the intensity slightly exceeds the value of I_{th} with the growth of the thickness of the induced-transparent layer, appearing at the depth $H_0 =$

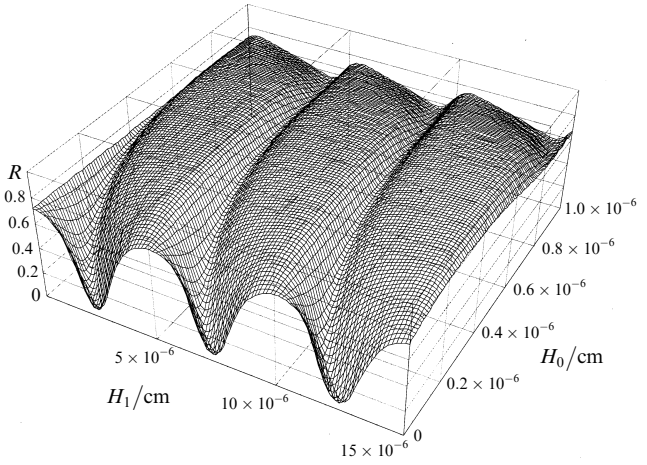

Figure 3. Reflection coefficient of the target versus thickness of the near-surface non-transparent H_0 and induced-transparent H_1 layers.

0.8×10^{-6} cm, the reflection coefficient increases, at first, from $R_0 = 0.72$ to 0.84 for $H_1 = 2 \times 10^{-6}$ cm, and then decreases to 0.65 for $H_1 = 5 \times 10^{-6}$ cm, following which a similar dependence repeats with the period $\Delta H_1 = 5.6 \times 10^{-6}$ cm. In the case when the induced-transparent layer appears at the depth $H_0 = 1.1 \times 10^{-6}$ cm, the reflection coefficient at first decreases from 0.72 to 0.57 for $H_1 = 4 \times 10^{-6}$ cm with the increase of the transparent-layer thickness, and then increases to 0.74 for $H_1 = 5.5 \times 10^{-6}$ cm (see Fig. 3).

Thus, the behaviour of the reflection coefficient during the propagation of the induced-transparency front essentially depends on the depth, at which the induced-transparent layer appears, i.e., on the position of the maximum of the temperature profile at the instant when the temperature of the induced transparency is reached. For the fixed value of the incident intensity the position of the maximum of the temperature profile is determined by the value $y = \alpha\chi/V$ (i.e. the lower is the value of y, the closer to the surface is the temperature maximum). Such behaviour of R in case of the radial intensity distribution in the bounded laser pulse leads to the radial dependence of the reflection coefficient and appearance of respective interference rings.

It is obvious that the presence of the plasma torch can impede the direct observation of such behaviour of the reflection coefficient. From this point of view, most preferable is the use of the regimes of evaporation with induced transparency, which are close to the stationary regime and require lower values of intensity than those in Ref. [17].

Fig. 4 shows the dependences of the plasma formation time on the intensity of the incident radiation for different initial temperatures and vapour concentrations at the outside boundary of the Knudsen layer, which were obtained with the code described in Ref. [27]. For $M = 1$ the temperature and concentration of vapour at the outside boundary of the Knudsen layer are, respectively, $0.63T_s$ and $0.32n_s$, where the concentration n_s of saturated vapours at the surface temperature T_s is determined by formulae $n_s = p_s/(kT_s)$ and (3). As is seen from Fig. 4, the threshold value of the intensity required for plasma formation is significantly greater than the above-calculated values of intensities typical for the stationary regime, which allows us to hope for the realisation of the stationary regime of evaporation with induced transparency without plasma formation.

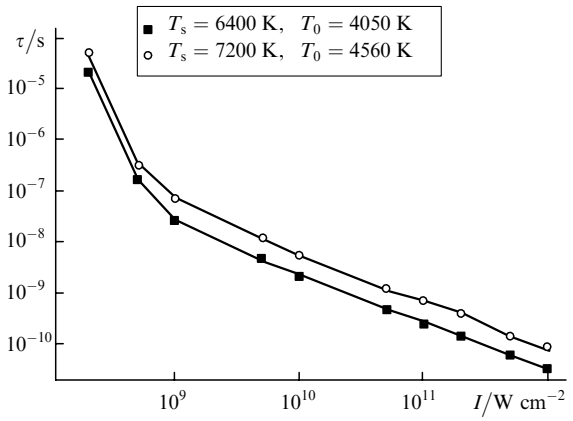

Figure 4. Time of plasma formation on the surface of the silicon target as a function of the incident radiation intensity for different temperatures of the target surface T_s.

4. Influence of induced transparency on a photoacoustic signal

In the stationary regime of evaporation without the induced transparency, the contribution of the evaporation pressure p_v, depending on the surface temperature T_s, to the total recoil pressure turns out to be significantly greater than the contribution resulting from variation of the density of the heated layer of condensed matter. The latter one can be estimated by formula $\Delta p \sim V^2\Delta\rho$, where $\Delta\rho = \rho(T_s) - \rho_\infty$ is the difference between densities on the surface and in the interior matter [12]. In case of the induced transparency, this formula contains the induced-transparency front velocity V_1 instead of V, and $\Delta\rho = \rho(T_b) - \rho_\infty$. For definiteness, further we will assume that there is no density jump at the induced-transparency front.

In the case of induced transparency at sufficiently high intensities, the induced-transparency front and melting front, related to the first, can move with the velocity V_1, which significantly exceeds the evaporation front velocity V. According to the data of Ref. [17], the transparent front velocity V_1, estimated as the ratio of the crater depth $H = 3 \times 10^{-3}$ cm to the pulse duration $\tau = 3$ ns, is of the order of the velocity of sound in condensed phase $V_1 \sim 10^6$ cm s^{-1}, i.e., the value of the additional pressure Δp can exceed the value of evaporation pressure even for relatively small $\Delta\rho$ [12].

To calculate the photoacoustic signal during the irradiation of the silicon target by the laser pulse with the Gaussian profile and duration $\tau = 3$ ns, the Lastec 1.1 program package [28] was used. This package provides the joint solving of one-dimensional continuity, Euler, and heat conduction equations for the compressible medium and volume absorption of the laser radiation by the target matter. The process of heat conduction in given calculations was assumed to be quasi-equilibrium, i.e., we neglected the difference between the electron and lattice temperatures, which, generally speaking, can noticeably change the dynamics of the process of heat transfer into interior target during irradiation by intense ultrashort laser pulses (see, for example, Refs [29, 30]).

The coefficient of thermal expansion in solid and liquid phases was taken equal to $\beta = 3 \times 10^{-6}$ K^{-1}. The total change in the target density at the induced-transparency front resulting from melting and thermal expansion was $\Delta\rho = \rho(T_b) - \rho_\infty = -0.25$ g cm^{-3}. The rest data on the silicon target were taken the same as in the above-mentioned calculations of the stationary temperature profile. Interference effects were, for simplicity, not taken into account in this calculation, inasmuch as possible non-monotonicity of the behaviour of photoacoustic signal connected with interference effects is characterised by very short periods of time (less than 1 ns). The average change of the reflection coefficient caused by the appearance of the induced-transparent layer was not taken into account as well, i.e., the incident radiation was assumed to be totally absorbed.

The time dependences of the photoacoustic signal for different values of the incident intensity are given in Fig. 5. After obtaining the induced transparency, the temperature on the surface and related evaporation pressure cease to increase within the sufficiently wide intensity range. The increase in the total pressure p_{pa} within this area is essentially connected with the velocity of the induced-transparency front. At the intensity $I = 0.5 \times 10^9$ W cm^{-2}

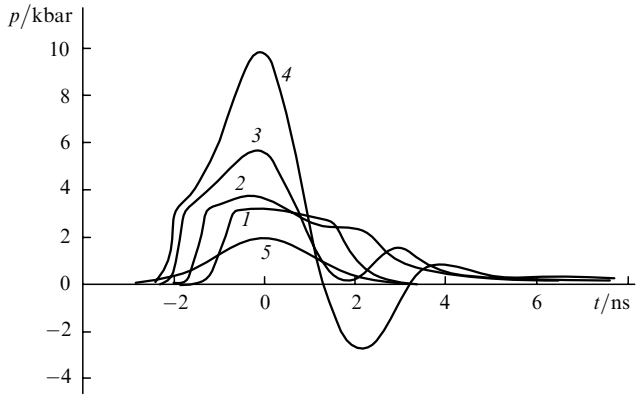

Figure 5. Total recoil pressure as a function of time for $I = 0.5 \times 10^9$ (*1*), 1×10^9 (*2*), 2×10^9 (*3*), 3×10^9 W cm^{-2} (*4*); (*5*) normalised laser (Gaussian) pulse.

[curve (*1*)], slightly exceeding the induced-transparency threshold, the transparent front velocity becomes small as compared with the velocity of sound, and the contribution $\Delta p_{\text{pa}} = p_{\text{pa}} - p_{\text{v}}$ of the photoacoustic signal, related to the movement of the transparent front, to the total pressure signal p_{pa} becomes also small. As the intensity increases, the contribution Δp_{pa} to the total recoil pressure grows. At the intensity $I = 2 \times 10^9$ W cm^{-2} [curve (*3*)] the peak value of Δp_{pa} becomes equal to the corresponding peak value of the evaporation pressure $p_{\text{v}}^{\max} \sim 3$ kbar, while at the intensity $I = 3 \times 10^9$ W cm^{-2} [curve (*4*)] it exceeds the value of $p_{\text{v}}^{\max}$ by more than a factor of three.

Fig. 6 demonstrates the dependence of maximum (over the time of interaction with the pulse) values of Δp_{pa} on the laser radiation intensity. Assuming that the profile of the density distribution with the drop $\Delta\rho$ remains constant, we can obtain the following expression [12] for the photoacoustic signal caused by the movement of this profile in the matter:

$$\Delta p_1 = \Delta\rho(V^2 + z_{\text{f}}\dot{V}), \tag{10}$$

where z_{f} и $\dot{V}$ represent, respectively, the position and acceleration of the density drop front. The maximum value Δp_1, obtained from the dynamics of the melting front, is in sufficiently good agreement with Δp_{pa}, calculated without the assumption of the invariability of the density distribution profile. For comparison, the intensity dependence of the parameter $\Delta\rho V_{\max}^2$, where $V_{\max}$ is the maximum (over the pulse duration) melting front velocity, is shown in Fig. 6. In this case, the difference between Δp_{pa} and $\Delta\rho V_{\max}^2$ turns out to be more noticeable, which is mainly connected with the time discrepancy of the signal maximum and the maximum of the velocity $V_{\max}$ as well as with the invalidity of the assumption of constant density distribution profile.

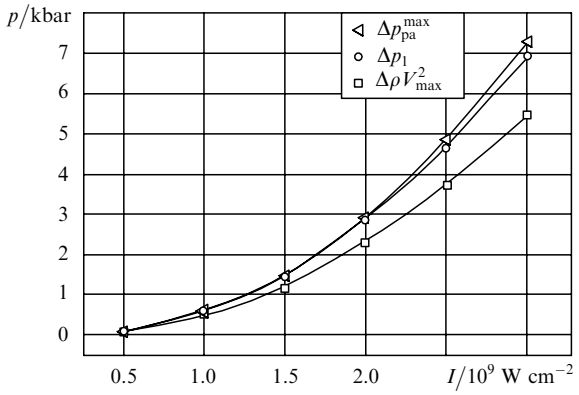

Figure 6. Maximum values of photoacoustic signal Δp_{pa} and parameters Δp_1, $\Delta\rho V^2$ versus laser pulse intensity.

Fig. 7 shows, for comparison, the total signal of the recoil pressure [curve (*1*)], evaporation pressure [curve (*2*)], photoacoustic signal Δp_{pa} [curve (*3*)], and Δp_1 [curve (*4*)] versus time for the laser pulse intensity $I = 2 \times 10^9$ W cm^{-2}. As is seen from Fig. 7, Δp_1 provides not only close approximation of maximum values of the photoacoustic signal, but also a sufficiently correct description of its temporal behaviour. Let us note that the slight decrease of 0.9 kbar in evaporation pressure [curve (*2*)] during lifetime of the induced-transparent layer is caused by the decrease of 300 K in surface temperature due to the reduction of the heat supply of the evaporation front. A sufficiently good agreement between Δp_1 and Δp_{pa} makes it possible to use the photoacoustic signal in the experiment in order to find the induced-transparent matter density for the determined velocity V. An independent measurement of V can be realised, for example, by registering the melting front velocity according to the behaviour of the probe infrared radiation, which is directed from the reverse of the target to the melting front and reflects from the latter.

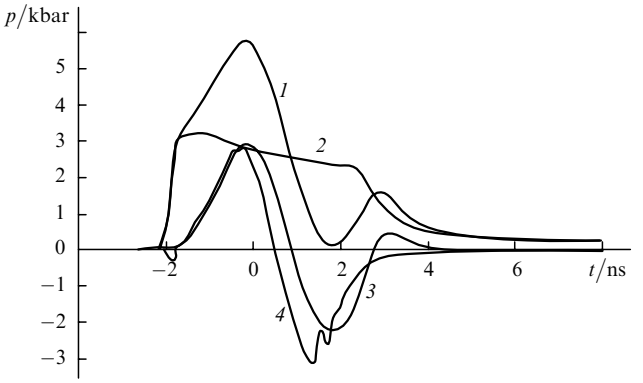

Figure 7. Total recoil pressure signal (*1*), evaporation pressure (*2*), photoacoustic signal Δp_{pa} (*3*), and parameter Δp_1 (*4*) versus time for laser pulse intensity $I = 2 \times 10^9$ W cm^{-2}.

As far as crystalline silicon transforms into metal upon melting and its density increases, $\Delta\rho$ can, in general, have different signs depending on the ratio of contributions of density variations caused by melting and thermal expansion under heating to T_{b}. However, the case $\Delta\rho > 0$ seems to be less probable, than the case $\Delta\rho < 0$, when the density of the induced-transparent matter is lower than the initial solid-state density. At the same time, both cases can be realised at the melting front depending on the material: thus, for example, the density of germanium, silicon, and bismuth increases under melting, while that of the most other metals decreases. The results of the respective calculations of the photoacoustic signal in cases of $\Delta\rho > 0$ and $\Delta\rho < 0$ at the melting front will be presented further.

5. Restrictions connected with the metastable-phase stability

The above-described model of the laser evaporation taking into account the induced transparency assumes that the appearing superheated metastable phase is thermodynamically stable at time periods of the order of laser pulse duration. Within the framework of such an approach, it is necessary to take into account the particularities of the behaviour of the heat conductivity and heat capacity near the boundary of the extreme superheating (spinodals) [8, 12] because the maximum of the temperature profile in the model with constant coefficients can exceed the critical temperature. In the opposite limit, the periodic volume boilings [7, 10, 12] can take place during the interaction with the laser pulse.

The assumption of the existence of a one-dimensional evaporation regime with the induced transparency is connected not only with the problem of the thermodynamic stability of the superheated metastable phase, but also with the problem of the morphological stability of the plane evaporation front [12, 31–33].

In the case of volume absorption with the coefficient $\alpha = 100\ \mathrm{cm}^{-1}$, considered in Ref. [32], the maximum value of the increment of the evaporation front instability is equal to $\gamma_{\max} = 1\ \mathrm{ns}^{-1}$ for the wave number $k_{\max} = 20.8\ \mu\mathrm{m}^{-1}$ and Mach number $M = 0.7$ in the flow of evaporated matter. We should bear in mind that these estimates relate to the case $\alpha = \mathrm{const}$ and $\chi = \mathrm{const}$, while in the model, which we consider, a near-surface non-transparent layer exists, wherein the values of α and χ are different from those in the induced-transparent layer. In general, more analysis is required to resolve the question of the stability of the evaporation front within the bounds of such model.

6. Conclusions

Thus, when the superheated metastable phase of the induced-transparent matter is sufficiently thermodynamically stable, the stationary regime of the developed evaporation with the plane front can probably exist during the time of about 10^{-8} s. The realisation of such a regime within the millisecond range seems to be unlikely. The laser radiation intensities required to maintain the stationary regime are substantially lower than those used in Ref. [17]. The decrease in the laser radiation intensity will allow one to avoid plasma torch formation near the target surface and provide additional possibilities for applications of the optical diagnostics of the irradiated surface. Estimates given in this work show that the appearance of the induced-transparent layer does not necessary lead to the direct decrease in reflectivity, the behaviour of which turns out to be more complicated. In case of the 'semi-stationary' regime, the dependence of the thickness of the induced-transparent layer on the laser pulse duration should be approximately linear, and this fact can be exploited as one of experimental indications of realisation of such regime. The induced transparency can exhibit most obviously in a photoacoustic effect, which usually is registered by the pressure sensor from the reverse side of the target [12, 16]. The value of contribution to the total recoil pressure connected with the movement of the induced-transparent front can exceed the evaporation pressure when the surface temperature $T_s \sim T_b$. In the same way one can register the increase in pressure connected with the onset of the explosive boiling of the metastable superheated phase. The observation of the above-described particularities of the induced transparency manifestation can allow one to make a more definite conclusion about the realisation of this effect in specific experiments.

Acknowledgements. The authors thank I.N. Kartashov for his attention to this work and useful discussions.

References

1. Landau L.D., Zel'dovich Ya.B. *Zh. Eksp. Teor. Fiz.*, **14**, 32 (1944).
2. Batanov V.A., Bunkin F.V., Prokhorov A.M., Fedorov V.B. *Zh. Eksp. Teor. Fiz.*, **36**, 311 (1973).
3. Karapetyan R.V., Samokhin A.A. *Kvantovaya Elektron.*, **1**, 2053 (1974) [*Sov. J. Quantum Electron.*, **4**, 1141 (1974)].
4. Bunkin F.V. *Kvantovaya Elektron.*, **1**, 2055 (1974) [*Sov. J. Quantum Electron.*, **4**, 1143 (1974)].
5. Shilov Yu.I. *Fiz. Tverd. Tela*, **19** (7), 1966 (1977).
6. Skripov V.P. *Metastable Liquids* (New York: Halsted, 1974).
7. Kozlov B.M., Samokhin A.A., Uspenskii A.B. *Kvantovaya Elektron.*, **2**, 2061 (1975) [*Sov. J. Quantum Electron.*, **5**, 1120 (1975)].
8. Samokhin A.A., Uspenskii A.B. *Zh. Eksp. Teor. Fiz.*, **46**, 543 (1977).
9. Korotchenko A.I., Popov N.I., Samokhin A.A. *Phys. Lett. A.*, **73**, 393 (1979).
10. Karlov N.V., Krynetskii B.B., Mishin V.A., Samokhin A.A. *Pis'ma Zh. Eksp. Teor. Fiz.*, **19**, 68 (1974).
11. Luthy W., Affolter K., Fuhrer M. *Phys. Lett. A*, **75**, 60 (1979).
12. Samokhin A.A. *Trudy IOFAN*, **13**, 1 (1990).
13. Miotello A., Kelly R. *Appl. Phys. A*, **69**, 67 (1999).
14. Bulgakova N.M., Bulgakov A.V. *Appl. Phys. A.*, **73**, 199 (2001).
15. Craciun V. et al. *Appl. Surf. Sci.*, **186**, 288 (2002).
16. Xu X., Song K. *Appl. Phys. A*, **69**, 869 (1999).
17. Yoo J.H., Jeong S.H., Greif R., Russo R.E. *J. Appl. Phys.*, **88** (3), 1638 (2000); Yoo J.H., Jeong S.H., Mao X.L., Greif R., Russo R.E. *Appl. Phys. Lett.*, **76** (6), 783 (2000).
18. Craciun V. *Appl. Phys. Lett.*, **79** (3), 442 (2001).
19. Yoo J.H., Jeong S.H., Greif R., Russo R.E. *Appl. Phys. Lett.*, **79** (3), 444 (2001).
20. Sokolowski-Tinten K., Bialkowski J., Cavalleri A., Von der Linde D., Oparin A., Meyer-ter-Vehn J., Anisimov S. *Phys. Rev. Lett.*, **81** (1), 224 (1998).
21. Inogamov N.A., Oparin A.M., Petrov Yu.V., Shaposhnikov N.V., Anisimov S.I., Von der Linde D., Meyer-ter-Vehn J. *Pis'ma Zh. Eksp. Teor. Fiz.*, **69**, 284 (1999).
22. Sokolowski-Tinten K., Von der Linde D. *Appl. Surf. Sci.*, **154/155**, 1 (2000).
23. Sokolowski-Tinten K. et al. *Phys. Rev. Lett.*, **87**, 225701 (2001).
24. Lu Q., Mao S., Mao X., Russo R. *Appl. Phys. Lett.*, **80** (17), 3027 (2002).
25. Andreev S.N., Samokhin A.A. *Kr. Soobshch. Fiz. FIAN*, (12), 12 (2001).
26. Mazhukin V.I., Prudkovskii P.A., Samokhin A.A. *Matematicheskoe modelirovanie*, **5**, 3 (1993).
27. Mazhukin V.I., Nossov V.V., Smurov I., Flamant G. *Surv. Math. Ind.*, (10), 45 (2001).
28. Mazhukin V.I., Nosov V.V. *Matem. Model.*, **6**, 3 (1994).
29. Kanavin A.P. et al. *Phys. Rev. B*, **57** (23), 14698 (1998).
30. Kanavin A.P. et al. *Izv. Ross. Akad. Nauk Ser. Fiz.*, **63** (4), 667 (1999).
31. Andreev S.N., Mazhukin V.I., Samokhin A.A. *Kr. Soobshch. Fiz. FIAN*, (9), 31 (2001).
32. Andreev S.N. et al. *Proc. Conf. IQEC/LAT-2002* (in press).
33. Kartashov I.N., Samokhin A.A. *Kr. Soobshch. Fiz. FIAN*, (10), 24 (2002).